

Water adsorption on rutile TiO₂(110) for applications in solar hydrogen production: A systematic hybrid-exchange density functional study

M. Patel,^{1,*} G. Mallia,¹ L. Liborio,¹ and N. M. Harrison^{1,2}¹*Thomas Young Centre, Department of Chemistry, Imperial College London, South Kensington, London, SW7 2AZ, UK*²*Daresbury Laboratory, Daresbury, Warrington, WA4 4AD, UK*

(Received 30 April 2012; published 5 July 2012)

Periodic hybrid-exchange density functional theory calculations are used to predict the structure of water on the rutile TiO₂(110) surface ($\Theta \leq 1$ ML), which is an important first step towards understanding the photocatalytic processes that occur in solar water splitting. A detailed model describing the water-water and water-surface interactions is developed by exploring thoroughly the adsorption energetics. The possible adsorption mode—molecular, dissociative, or mixed—and the binding energy are studied as a function of coverage and arrangement, thus separation, of adsorbed species. These dependencies (coverage and arrangement) have a significant influence on the nature of the interactions involved in the H₂O-TiO₂ system. The importance of both direct intermolecular and surface-mediated interactions between surface species is emphasized. Finally, to gain insight into the photooxidation of adsorbed species at the surface, the electronic structure of the predicted adsorbate-substrate geometries is analyzed in terms of total and projected density of states.

DOI: [10.1103/PhysRevB.86.045302](https://doi.org/10.1103/PhysRevB.86.045302)

PACS number(s): 68.43.Bc, 68.43.Fg, 82.30.Nr, 82.65.+r

I. INTRODUCTION

The storage and transport of hydrogen, the efficient conversion of hydrogen into electrical energy in fuel cells,^{1,2} and the production of hydrogen via photocatalytic water splitting^{3,4} are current challenges in the hydrogen economy. Water splitting over semiconductor materials, such as titanium dioxide (TiO₂), provides a carbon-free renewable route to hydrogen production.^{5–7} However, the required solar-to-fuel efficiencies have been unattainable at a reasonable cost,⁸ and there is ample motivation to enhance the photochemical conversion efficiency of the photocatalytic material. A dependency of photocatalytic activity on the surface facet has become evident from a number of experimental studies,^{9–12} though the reasons for this dependency are unknown (see Ref. 13 for proposed mechanisms). A clear atomistic understanding of water chemistry on transition metal oxide photocatalyst surfaces—a prerequisite for apprehending the correspondence between water adsorption properties and photocatalytic activity—has not yet been established; it is hoped that fundamental insight into the photocatalytic mechanism will facilitate the design of more efficient systems.

TiO₂ is a transition metal oxide that adopts a variety of crystal structures, three of which are rutile, anatase, and brookite. The (110) surface of rutile TiO₂ is the most stable among the rutile low-index surfaces,^{14–16} and is considered to be a quintessential model metal oxide system for the study of water chemistry. This surface has received considerable attention for its use in photochemical reactions,¹⁷ heterogeneous catalysis,¹⁸ sorbent technology,¹⁹ gas sensors,²⁰ and, in particular, photoelectrochemical solar energy conversion for the production of hydrogen²¹ and electricity.⁴

Generally speaking, a water molecule is able to bind to a surface molecularly or dissociatively. The former entails interaction of the intact molecule with the surface; the latter involves deprotonation of the water molecule and the formation of surface hydroxyls.¹⁴ An ongoing issue that has attracted much attention is the question of whether water molecules are

adsorbed molecularly or dissociatively on the rutile TiO₂(110) surface, and the conditions under which each mode of adsorption takes place. Surface x-ray diffraction studies²² have shown that when the surface is in contact with a liquid water film, a hydration layer forms in which adsorbate oxygen atoms occupy all surface fivefold-coordinated Ti sites. However, the crystal truncation rod (CTR) measurements performed could not unambiguously determine the coordinates of this hydration layer, so the definitive structure of adsorbates in the adsorbed water layer was not determined.^{13,22} The majority of experimental work supports the view that molecular adsorption dominates in the first layer of water ($\Theta \leq 1$ ML) on nearly perfect surfaces at low temperatures (<350 K), and that water dissociates only at oxygen vacancy sites.^{23–33} The evidence for this picture includes ultraviolet photoelectron spectroscopy (UPS) measurements by Kurtz *et al.*²³ of the nearly perfect (110) surface, which was interpreted in terms of molecular adsorption at monolayer coverage (1 ML) at 160 K, dissociative adsorption at low coverage (~ 0.1 ML) at 300 K, and suggested that the rate of dissociation is higher on defective surfaces. Two other UPS studies indicated dissociative adsorption at low coverage, but deduced that dissociation occurred only at oxygen vacancy defect sites.^{24,25} A study by Hugenschmidt *et al.*²⁶ showed a temperature-programmed desorption (TPD) peak at 275 K, which was assigned to molecular adsorption on the nearly perfect surface at 1 ML using work function measurements and x-ray photoelectron spectroscopy (XPS). Dissociative adsorption was assigned to a tail of this peak extending to 375 K at ~ 0.25 ML. Henderson²⁷ used high-resolution electron energy loss spectroscopy (HREELS) to assign a TPD peak at 270 K to monolayer states; the first layer of water was attributed to molecular adsorption [$\nu(\text{OH}) = 3420\text{--}3505$ cm⁻¹ and $\delta(\text{HOH}) = 1625$ cm⁻¹], and the study suggested that at 135 K, water was active for dissociation only at low coverage (~ 0.1 ML) and in the presence of structural defects [$\nu(\text{OH}) = 3690$ cm⁻¹]. A combined TPD and molecular beam scattering study by Brinkley *et al.*²⁹

came to similar conclusions: $<2\%$ of the molecules incident on the surface undergo dissociative adsorption on the defect-free surface at very low coverage (≤ 0.01 ML). As a sequel, the conclusions made from experimental studies vary notably in relation to the extent of dissociation on the nearly perfect surface at various temperatures.^{23,27,31} An alternative interpretation of this evidence, and, in particular, of the HREELS spectrum, was developed on the basis of first-principles molecular dynamics.³⁴ In the calculated hydrogen vibrational power spectrum, both water bond-bending $\delta(\text{HOH})$ and O-H stretching $\nu(\text{OH})$ signals were present. A broadened OH contribution was assigned to those species that participate in hydrogen bonding, and a sharp blue-shifted peak was due to the vibrations of the H in the terminal hydroxyl, which is not hydrogen bonded. This study proposed that molecular and dissociative water can coexist on the defect-free surface at 1 ML. Following this, a study by Walle *et al.*³⁵ presented experimental evidence for this, using photoemission measurements, demonstrating that the formation of a monolayer of water on a rutile $\text{TiO}_2(110)$ surface free from oxygen vacancy defects, at low temperature under UHV conditions, involves both molecular and dissociated water.

In contrast to experiment, the majority of theoretical studies indicate that the dissociation of water is energetically favoured on the defect-free rutile $\text{TiO}_2(110)$ surface at all coverages up to 1 ML.^{36–46} It should be noted, however, that many of these simulations are based on structural models characterized by either point group or translational symmetry constraints. Semiempirical tight-binding studies based on cluster models by Goniakowski *et al.* and Bredow *et al.* show favorable dissociative adsorption at all coverages,^{36–38} as do some early first-principles Hartree-Fock (HF) and density functional theory (DFT) studies.^{39,40} A first-principles molecular dynamics (MD) study by Lindan *et al.*,⁴⁷ using the generalized gradient approximation (GGA), employed a periodic slab approach to show that dissociation of water leads to stabilization at low coverages. In these calculations, all adsorbates are subject to symmetry constraints, so neighboring molecules are restricted to be at fixed orientation and separation. In Ref. 34, it was pointed out that translational symmetry must be relaxed to allow intermolecular interactions to be studied reliably at high coverage ($\Theta = 1$ ML). A later study by Lindan and Zhang,⁴⁶ using plane-wave pseudopotential DFT, predicted favorable dissociative adsorption over a range of coverages. They suggested that a barrier to dissociation explains why molecular adsorption is observed experimentally below 160 K, and that neighboring molecules lower this dissociation barrier through hydrogen bonding. The important role of intermolecular interactions has been stressed,^{34,46,48,49} suggesting a more complex picture at monolayer coverage, in which both molecular and dissociated water coexist on the surface, stabilized by a hydrogen bond. From the extensive literature on theoretical studies, it is clear that the adsorption energetics are very sensitive to intermolecular interactions, electronic structure methods, e.g., DFT functional adopted, and differences in computational models (see detailed review in Ref. 50).

The purpose of this study is to develop a better understanding of the $\text{H}_2\text{O}-\text{TiO}_2$ interactions involved in photocatalytic water splitting using the defect-free rutile $\text{TiO}_2(110)$ surface

as the model system. In order to study the behavior of water on this surface ($\Theta \leq 1$ ML), we have used hybrid-exchange DFT calculations with the B3LYP functional, which result in an accurate description of the energetics and the electronic structure of periodic systems,^{51–64} particularly for transition metal oxides, and, as implemented in the CRYSTAL code, are computationally efficient for large systems.⁶⁵ This approach aims to develop a detailed model of interactions for this surface, prior to uncovering the role of defects as well as dependence on surface facet: a thorough investigation of the energetics has been performed, and the method adopted facilitates the analysis of the interactions between adjacent adsorbates. The calculations can be separated into so-called “single-molecule” and “two-molecule” adsorption in which one and two molecules are adsorbed per surface unit cell, respectively. This terminology has been used in the present study in order to highlight the importance of breaking translational symmetry in intermolecular interactions as well as to be consistent with the language adopted in previous theoretical water adsorption studies.^{34,43,46–48,50,66} Molecular, dissociative and mixed adsorption modes are considered at each coverage and/or arrangement of adsorbates on the surface.

This paper is organized as follows. Section II contains the computational details. Results of DFT calculations are presented in Sec. III. The discussion begins with the calculated energetics and optimized geometries, followed by an analysis of the electronic structure of rutile $\text{TiO}_2(110)$ in contact with water. The focus of the discussion is the effect of varying coverage and adsorbate arrangement on the binding energy as well as the influence of intermolecular interactions. Section IV contains the conclusions drawn from this study.

II. COMPUTATIONAL DETAILS

All calculations have been performed using the CRYSTAL09 software package,^{67,68} based on the expansion of the crystalline orbitals as a linear combination of a local basis set (BS) consisting of atom-centered Gaussian orbitals. The titanium and oxygen atoms are described by a triple valence all-electron BS: an 86-411G** contraction (one s , four sp and two d shells) and an 8-411G* contraction (one s , three sp , and one d shells), respectively;⁶⁹ the most diffuse sp (d) exponents are $\alpha^{\text{Ti}} = 0.3297$ (0.26) and $\alpha^{\text{O}} = 0.1843$ (0.6) bohr⁻². These basis sets were developed in previous studies of the bulk and surface phases of titania in which a systematic hierarchy of all-electron basis sets was used to quantify the effects of using a finite BS.^{70,71} The hydrogen atom is described by two s and one p shells, corresponding to a 6-31G** contraction⁷²; the quality of the oxygen and the hydrogen BS in describing the water molecule is assessed in Appendix A.

Electronic exchange and correlation are approximated using the hybrid-exchange B3LYP functional. Matrix elements of the exchange and correlation potentials and the energy functional are integrated numerically on an atom-centered grid of points. The integration over radial and angular coordinates is performed using Gauss-Legendre and Lebedev schemes, respectively. A pruned grid consisting of 99 radial points and five subintervals with (146, 302, 590, 1454, 590) angular points has been used for all calculations (the XXLGRID option implemented in CRYSTAL09⁶⁷). This grid converges

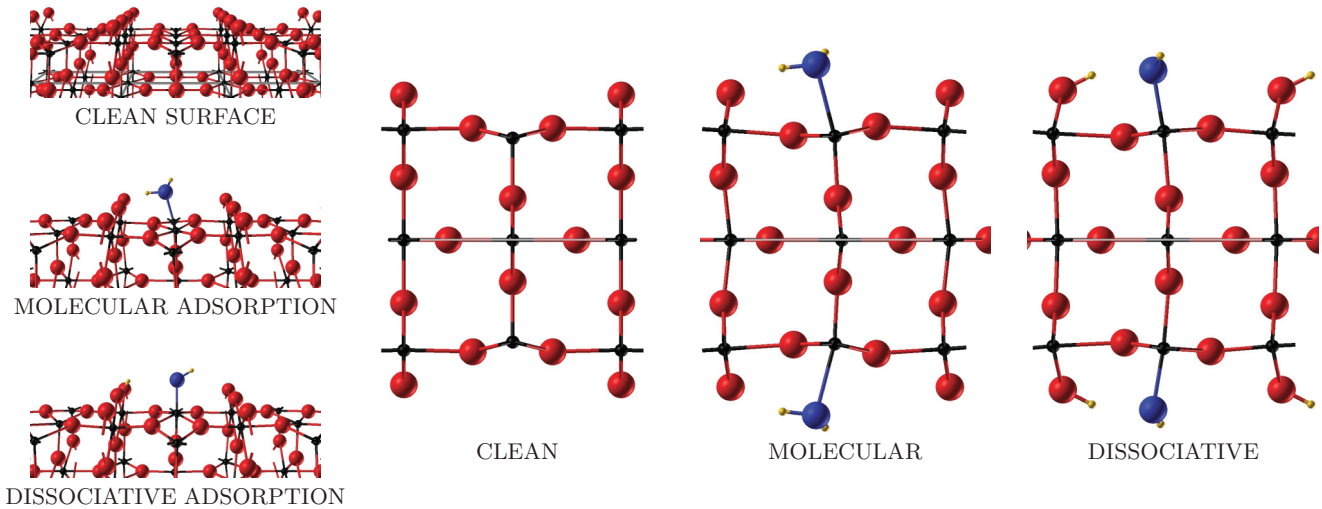


FIG. 1. (Color online) Optimized geometries of the rutile TiO₂(110) surface before and after adsorption of a water molecule. Structural changes can be seen in the surface atomic layers upon adsorption. Side views are along \mathbf{b}_{slab} , corresponding to the $[1\bar{1}0]$ direction of the bulk; the 1×1 surface unit cell is displayed ($\Theta = 1$ ML). O, Ti, adsorbate O and adsorbate H atoms are represented by red, black, blue, and yellow spheres, respectively. If viewed in black and white: O, Ti and H atoms appear as dark grey, black and light grey spheres, respectively.

the integrated charge density to an accuracy of about $\times 10^{-6}$ electrons per formula unit. The Coulomb and exchange series are summed directly and truncated using an overlap criterion with thresholds of 10^{-7} , 10^{-7} , 10^{-7} , 10^{-7} , and 10^{-14} as described previously.^{67,73} Reciprocal space sampling for the bulk structure was performed on a Pack-Monkhorst net with a shrinking factor $IS = 8$ along each periodic direction.

With regards to the surface,⁶⁸ a nine-atomic-layer (9AL) slab cut from the bulk has been used. In previous studies,^{34,46,74} single-molecule adsorption calculations using this slab size were performed; our results are in agreement with the reported relative stabilities of the adsorption modes (molecular versus dissociative) for 9, 15, and 21-atomic-layer slabs. The convergence with respect to slab thickness can be analyzed by considering the percentage difference between 9AL and 15AL systems. For instance, using a 1×1 cell ($\Theta = 1$ ML), the percentage differences between the energies for the 9AL and 15AL systems are 13% and 20% for the molecular and dissociative adsorption modes, respectively. However, since it is the relative stability that we are interested in, it has to be noticed that in the present work, the energy difference between the molecular (lowest in energy) and dissociative adsorption modes (see Sec. III A) is 0.16 eV for the 9AL slab, and 0.25 eV for the 15AL slab. These correspond to percentages of 16% and 19%, respectively, with respect to the molecular adsorption energy. The electronic structure is unaffected by an increase in slab thickness from 9AL to 15AL, in terms of the contributions to the valence and conduction bands in the projected density of states. In the current work, using a 9AL slab has allowed a systematic, detailed and computationally viable study of the coverage and arrangement of adsorbates. The shrinking factors [8, 8], [4, 8], [4, 8], [2, 8], [8, 4], and [4, 4] were adopted along the two periodic directions for 1×1 , 2×1 , 3×1 , 4×1 , 1×2 , and 2×2 surface unit cells, respectively, in order to ensure consistent k -space sampling. The self-consistent field procedure was converged up to a tolerance in the total energy of $\Delta E = 1 \times 10^{-7} E_h$ per unit cell.

The predicted structural parameters, with the deviation from those observed⁷⁵ in parenthesis, are $\mathbf{a}_{\text{bulk}} = \mathbf{b}_{\text{bulk}} = 4.639 \text{ \AA}$ (1.1%), $\mathbf{c}_{\text{bulk}} = 2.979 \text{ \AA}$ (0.9%), and $u = 0.306$ (0.5%). This structure is consistent with that predicted in previous calculations.^{53,56,71,76} Since the slab is cut from the optimized bulk, the corresponding lattice parameters are $\mathbf{a}_{\text{slab}} = 2.979 \text{ \AA}$ ([001] direction of the bulk) and $\mathbf{b}_{\text{slab}} = 6.561 \text{ \AA}$ ($[1\bar{1}0]$ direction of the bulk). Structural optimization was performed, relaxing all atoms of the adsorbate(s) and the slab, using the Broyden-Fletcher-Goldfarb-Shanno scheme, as implemented in CRYSTAL09.⁶⁷ Convergence was determined from the root-mean square (rms) and the absolute value of the largest component of the forces. The thresholds for the maximum and the rms forces (the maximum and the rms atomic displacements) have been set to 0.00045 and 0.00030 (0.00180 and 0.0012) in atomic units. Geometry optimization was terminated when all four conditions were satisfied simultaneously. Projection of density of states was carried out following a Mulliken analysis.

The binding energy (BE) per molecule of the adsorbate-substrate system was computed with respect to the isolated molecule and the clean surface. The counterpoise correction to the binding energy was applied to take into account the basis set superposition error (BSSE), details of which are documented in Refs. 77 and 78. In addition, it should be noted that one molecule was adsorbed on each side of the slab.

III. RESULTS AND DISCUSSION

Firstly, the geometry and energetics for single-molecule adsorption (one molecule adsorbed per surface unit cell) are discussed in Sec. III A. An analysis of the energetics for two-molecule adsorption (two molecules adsorbed per surface unit cell) is given in Sec. III B. The electronic structure for the rutile TiO₂(110) surface in contact with water is then presented in Sec. III C.

TABLE I. Displacements (Δx , Δy , and Δz in Å) of atoms in the uppermost three atomic layers, with respect to the clean relaxed rutile $\text{TiO}_2(110)$ surface geometry, in molecular and dissociative single-molecule adsorption. x , y , and z correspond to the $[001]$, $[1\bar{1}0]$, and $[110]$ directions of the bulk, respectively. The 1×1 and 2×2 supercell cases are considered here. The corresponding coverage Θ is also indicated. The labels $\text{O}_{3c:1}$ and $\text{O}_{3c:2}$ refer to the four equatorial oxygen atoms of Ti_{5c} , the former(latter) being to the left(right) of Ti_{5c} in Fig. 1.

	Molecular						Dissociative					
	1×1			2×2			1×1			2×2		
	$\Theta = 1$			$\Theta = 1/4$			$\Theta = 1$			$\Theta = 1/4$		
	Δx	Δy	Δz	Δx	Δy	Δz	Δx	Δy	Δz	Δx	Δy	Δz
Ti_{5c}	0.02	0.07	0.04	-0.01	0.07	0.13	-0.08	-0.13	0.18	0.00	0.03	0.55
Ti_{6c}	0.24	0.07	-0.05	0.02	-0.01	-0.04	-0.01	-0.16	-0.15	0.06	0.06	-0.06
O_{2c}	0.13	0.24	0.04	0.01	0.13	0.01	-0.01	0.13	0.11	0.00	0.03	0.17
$\text{O}_{3c:1}$	0.12	0.12	0.04	0.00	0.00	0.03	-0.01	0.07	-0.03	-0.01	0.05	0.01
$\text{O}_{3c:2}$	0.12	0.05	-0.24	0.01	-0.02	0.03	-0.01	-0.10	-0.3	0.03	0.02	-0.05

A. Single-molecule water adsorption: Geometry and energetics

The clean rutile $\text{TiO}_2(110)$ surface, characterized by the fivefold-coordinated titanium (Ti_{5c}) and the twofold-coordinated “bridging” oxygen atoms (O_{2c}), is shown in Fig. 1 together with models representing the molecular and dissociative adsorption of water. In both modes, it is the Ti_{5c} and O_{2c} terminal ions that interact with adsorbing species. In the dissociative case, the adsorption of OH onto Ti_{5c} forms a terminal hydroxyl (TH), and the H atom, detached from H_2O , bonds to the nearest O_{2c} resulting in a bridging hydroxyl (BH).

The surface undergoes significant structural changes upon water adsorption. These changes can be observed in the relaxed geometries shown in Fig. 1, and analyzed by considering the atomic displacements in Table I. To investigate the coverage dependence of water adsorption, supercells of different sizes and shapes were used. A 1×1 unit cell can be extended in the $[001]$ and $[1\bar{1}0]$ directions to form 2×1 , 3×1 , 4×1 , 1×2 , and 2×2 unit cells, decreasing the coverage and increasing the distance between adsorbates. From the relaxed geometry of the clean 1×1 surface, it can be seen that the Ti_{5c} moves inwards, specifically by 0.14 Å, to increase effective coordination with neighbouring O ions. Upon adsorption, in both molecular and dissociative modes, the Ti_{5c} moves outwards: this is expected as the adsorption of OH or H_2O restores the octahedral coordination of the Ti ion. The displacement Δz of Ti_{5c} is larger when water dissociates, which can be explained by a greater electrostatic interaction of the terminal OH^- with the Ti^{4+} ion, compared to molecular adsorption. This effect is more significant in the 2×2 supercell ($\Delta z = 0.18$ Å for 1×1 and

$\Delta z = 0.55$ Å for 2×2), suggesting that when the OH^- species are further apart, surface distortions allow extra movement of Ti_{5c} . Conversely, the sixfold-coordinated titanium atom (Ti_{6c}) in the second atomic layer moves into the slab while O_{2c} moves outwards; this is more apparent for the dissociative adsorption (in the 1×1 cell, Ti_{6c} $\Delta z = -0.05$ Å for molecular and $\Delta z = -0.15$ Å for dissociative; O_{2c} $\Delta z = 0.04$ Å for molecular and $\Delta z = 0.11$ Å for dissociative). This is consistent with a simple electrostatic picture in which the adsorption of H onto the O_{2c} atom (forming the bridging hydroxyl BH: O_{2c}H^-) is expected to decrease the attractive Coulombic interaction between O_{2c}^{2-} and Ti_{6c}^{4+} , which in turn would be attracted by the bulklike oxygen atoms O^{2-} below. The displacements in x , y , and z of the four equatorial oxygen atoms of Ti_{5c} (labelled $\text{O}_{3c:1}$ and $\text{O}_{3c:2}$, see Table I) indicate that the packing of the surface TiO_6 octahedra is also affected by the water adsorption: the main axis of the octahedron is tilted with respect to the clean surface, as shown in Fig. 1, allowing the attractive interactions occurring at the surface to be maximised.

The distances between Ti_{5c} and the oxygen of the adsorbate (O_{ads}) for both adsorption modes are reported in Table II. By comparing these to the apical Ti-O bond length in bulk rutile— $d(\text{TiO}_{\text{ap}}) = 2.009$ Å—the larger Δz displacement of Ti_{5c} reported above can be rationalized further. The $\text{Ti}_{5c}\text{O}_{\text{ads}}$ bond lengths in the dissociative mode [$d(\text{Ti}_{5c}\text{O}_{\text{ads}}) = 1.8\text{--}1.9$ Å] are closer in value to the bulk than those in the molecular mode [$d(\text{Ti}_{5c}\text{O}_{\text{ads}}) = 2.2\text{--}2.3$ Å], indicating a greater ionicity of O_{ads} in the former. In Table II, the various O-H distances are also given. The bridging hydroxyl, $d(\text{O}_{2c}\text{H}_{\text{ads}})$, and the

TABLE II. $\text{Ti}_{5c}\text{O}_{\text{ads}}$ and various O-H bond lengths (Å) in molecular and dissociative single-molecule adsorption on the rutile $\text{TiO}_2(110)$ surface.

Supercell size	Coverage Θ	Molecular	Dissociative			
		$d(\text{Ti}_{5c}\text{O}_{\text{ads}})$	$d(\text{Ti}_{5c}\text{O}_{\text{ads}})$	$d(\text{O}_{2c}\text{H}_{\text{ads}})$ BH	$d(\text{O}_{\text{ads}}\text{H}_{\text{ads}})$ TH	$d(\text{H}_{\text{BH}}\text{O}_{\text{TH}})$ Hydrogen bond
1×1	1	2.266	1.903	0.992	0.974	1.840
2×1	1/2	2.184	1.821	0.970	0.967	2.422
3×1	1/3	2.177	1.803	0.967	0.968	2.686
4×1	1/4	2.173	1.801	0.967	0.968	2.694
1×2	1/2	2.251	1.904	0.995	0.975	1.819
2×2	1/4	2.190	1.804	0.968	0.969	2.692

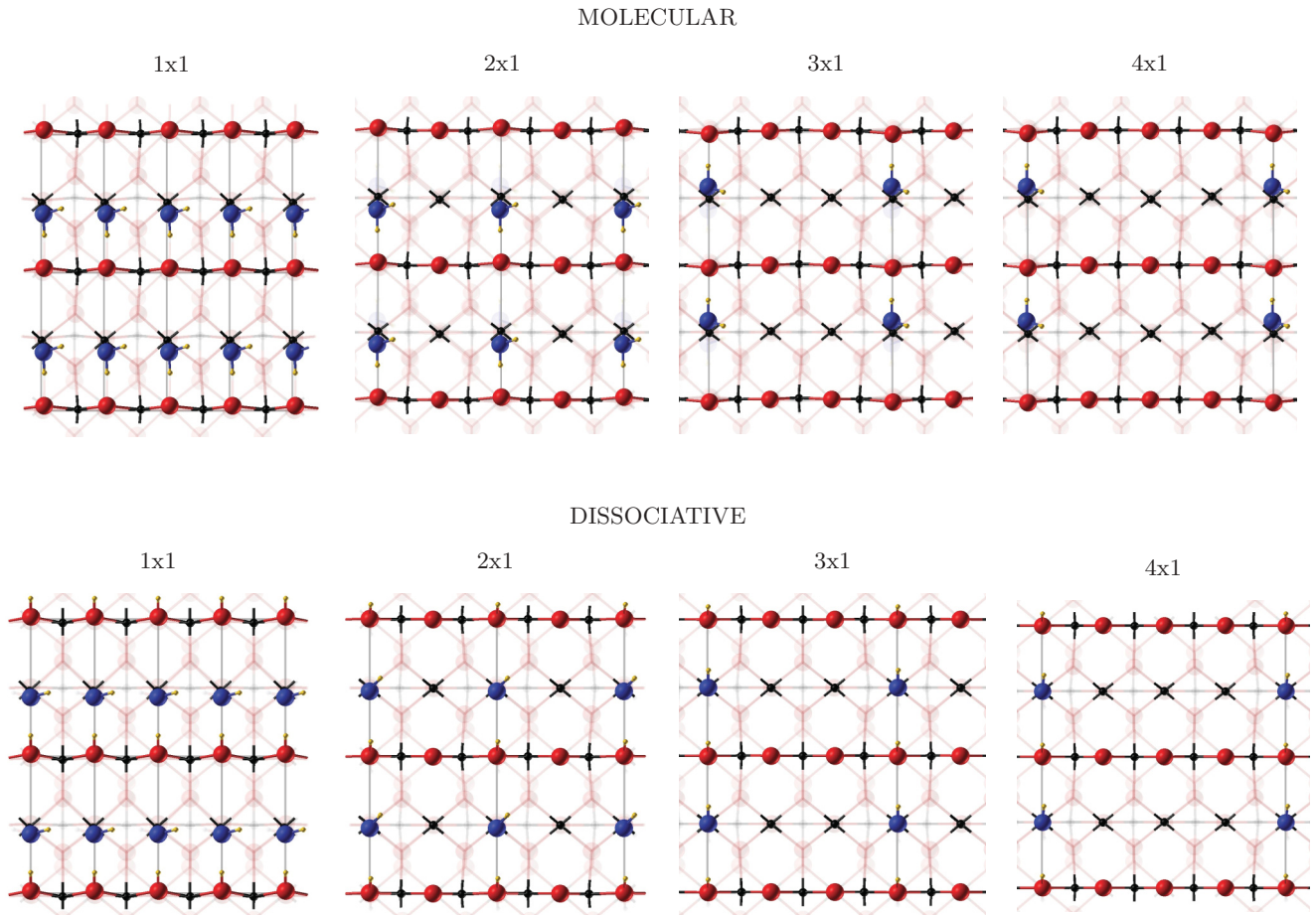


FIG. 2. (Color online) Top views of the adsorbate-substrate system in single-molecule adsorption, illustrating the effect of varying coverage ($\Theta = 1$ to $1/4$ ML) in \mathbf{a}_{slab} . The Ti atoms of the two uppermost atomic layers, bridging O atoms, alongside those atoms belonging to the adsorbate, are opaque, whereas lower layers are translucent. O, Ti, adsorbate O, and adsorbate H atoms are represented by red, black, blue, and yellow spheres, respectively. The surface unit cell in each case is represented by a grey line. If viewed in black and white: O, Ti and H atoms appear as dark grey, black and light grey spheres, respectively.

terminal hydroxyl, $d(\text{O}_{\text{ads}}\text{H}_{\text{ads}})$, are characterized by very similar bond lengths, close to the O-H bond length in the gas-phase water molecule, $d(\text{OH}) = 0.964 \text{ \AA}$ (see Appendix A for a comparison between calculated and experimental data for H_2O). In addition, the hydrogen bond distance between the hydrogen atom of BH and the oxygen atom of TH, $d(\text{H}_{\text{BH}}\text{O}_{\text{TH}})$, is displayed. When decreasing the coverage by increasing the size of the supercell in \mathbf{a}_{slab} , corresponding to the $[001]$ direction of the bulk, there is a change in the orientation of TH, which can be seen in Fig. 2. The distance $d(\text{H}_{\text{BH}}\text{O}_{\text{TH}})$ increases from 1.84 to 2.69 \AA ; this geometric response and change in hydrogen bond distance becomes significant in the analysis of water adsorption energetics presented below.

The binding energy (BE) of the $\text{H}_2\text{O}-\text{TiO}_2(110)$ system with respect to the isolated molecule and the clean surface⁷⁸ is given per molecule in Table III as a function of the coverage Θ , for both the molecular and dissociative adsorption of water. The corresponding adsorption geometries are illustrated in Figs. 2 and 3. The BE is negative for all cases considered: water binds readily to the surface at all coverages. Excluding the 1×1 and 1×2 periodicities for the moment, dissociation of water is more stable than molecular adsorption; a possible reason for this is the formation of hydrogen bonding interactions between

the bridging and terminal hydroxyls, in agreement with previous work.^{34,46} The adsorption becomes sequentially more favourable as the coverage decreases: increasing the separation between adsorbates along \mathbf{a}_{slab} from 5.959 to 8.939 to 11.918 \AA

TABLE III. The binding energies (BE) per molecule of the adsorbate-substrate system with respect to the clean surface and the isolated molecule⁷⁸ are shown for relaxed geometries in single-molecule adsorption. Binding energies for both the molecular and dissociative modes of adsorption are shown as a function of coverage, Θ . Each supercell corresponds to a particular geometrical configuration.

Supercell size	Coverage Θ	BE/eV	
		Molecular	Dissociative
1×1	1	-0.98	-0.82
2×1	$1/2$	-0.92	-1.21
3×1	$1/3$	-0.92	-1.40
4×1	$1/4$	-0.97	-1.46
1×2	$1/2$	-1.06	-0.87
2×2	$1/4$	-1.04	-1.33

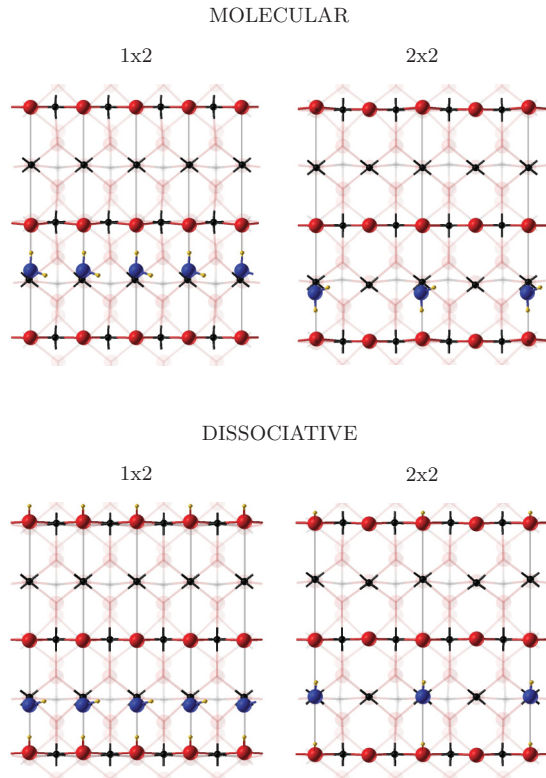


FIG. 3. (Color online) Top views of the adsorbate-substrate system in single-molecule adsorption in the 1×2 and 2×2 supercell cases. The Ti atoms of the two uppermost atomic layers, bridging O atoms, alongside those atoms belonging to the adsorbate, are opaque, whereas lower layers are translucent. O, Ti, adsorbate O, and adsorbate H atoms are represented by red, black, blue, and yellow spheres, respectively. The surface unit cell in each case is represented by a grey line. If viewed in black and white: O, Ti and H atoms appear as dark grey, black and light grey spheres, respectively.

lowers the BE by 0.19 and 0.06 eV, respectively. This suggests that the effective repulsive interactions between the adsorbed species are lowered as the separation is increased. This effect is much smaller for molecular adsorption: increasing the separation between adsorbed molecules along \mathbf{a}_{slab} from 5.959 to 8.939 Å does not affect the BE, and from 8.939 to 11.918 Å the BE is lowered by 0.05 eV. This indicates that interactions between surface hydroxyls along \mathbf{a}_{slab} are more pronounced and spread over a greater distance than those between adsorbed molecules. Additionally, the coverage-dependent stabilisation is evident from the $\text{Ti}_{5c}\text{-O}_{\text{ads}}$ bond lengths (see Table II), which presents an interesting correlation; the more negative the BE, the shorter the distance $d(\text{Ti}_{5c}\text{-O}_{\text{ads}})$.

The exceptions to these trends are the 1×1 and 1×2 periodicities in which the molecular adsorption is more stable. These systems are stabilised by the molecules being close enough to benefit from hydrogen bonding along the \mathbf{a}_{slab} direction (2.979 Å). Particularly strong interactions between neighboring terminal hydroxyls can be seen in the 1×1 and 1×2 dissociative systems; the hydroxyls have tilted to maximize the hydrogen bonding interactions [see Table II for $d(\text{H}_{\text{BH}}\text{O}_{\text{TH}})$ bond distances] and to avoid repulsion between parallel OH groups. It is important to note that along the

\mathbf{b}_{slab} direction (6.561 Å), the interactions are negligible; this can be seen by comparing the 1×1 and 1×2 periodicities in Table III,⁵⁶ but becomes more evident in the results of two-molecule adsorption energetics reported in Sec. III B.

When analyzing the results, one of the factors to be taken into account is the effect of the constraints imposed by point group and translational symmetry on the relaxation of the atomic structure. The calculations discussed here benefit from symmetry-breaking induced by the interactions between adsorbates at the surface; they contain two point group symmetry operators and refer to the lowest energy geometric states found. On the contrary, if the symmetry of the clean (110) surface is imposed, the system is constrained and the binding energy is higher by an energy within the range 0.15–0.85 eV. The effect of symmetry is analysed in Appendix B, which includes results presented in Ref. 79. The adsorption of two molecules per surface unit cell is expected to produce more negative binding energies compared to single-molecule adsorption results for equivalent atomic configurations, since there is a partial breaking of the translational symmetry constraints, and therefore more freedom for the atoms to relax. This expected effect on the stability is discussed further in Sec. III B.

B. Two-molecule water adsorption: Energetics

The adsorption of two molecules per surface unit cell allows a mixed molecular and dissociative adsorption mode

TABLE IV. The binding energies (BE) per molecule of the adsorbate-substrate system with respect to the clean surface and the isolated molecules⁷⁸ are presented for relaxed geometries in two-molecule adsorption. Binding energies for molecular (M), dissociative (D), and mixed (DM) adsorption modes are shown as a function of coverage, Θ . The labels a, b, and c represent different atomic configurations in the supercell, as described in the text; the notation _ represents an empty site in the cell.

Supercell size	Coverage Θ	BE/eV		
		Molecular	Dissociative	Mixed
2×1	1	-0.99	-0.85	-1.03
		MM	DD	DM
3×1	2/3	-0.95	-1.10	-1.15
		MM_	DD_	DM_
4×1	1/2	-0.98	-1.24	-1.20
		MM_	DD_	DM_
$4 \times 1_a$	1/2	-0.92	-1.20	-1.11
		M_M_	D_D_	D_M_
1×2	1	-1.00	-0.82	-0.89
		M	D	M
		M	D	D
$2 \times 2_a$	1/2	-1.06	-0.86	-1.09
		—	—	—
$2 \times 2_b$	1/2	-0.96	-1.22	-1.09
		M_	D_	M_
$2 \times 2_c$	1/2	-0.96	-1.23	-1.09
		_M	_D	_M
		M_	D_	D_

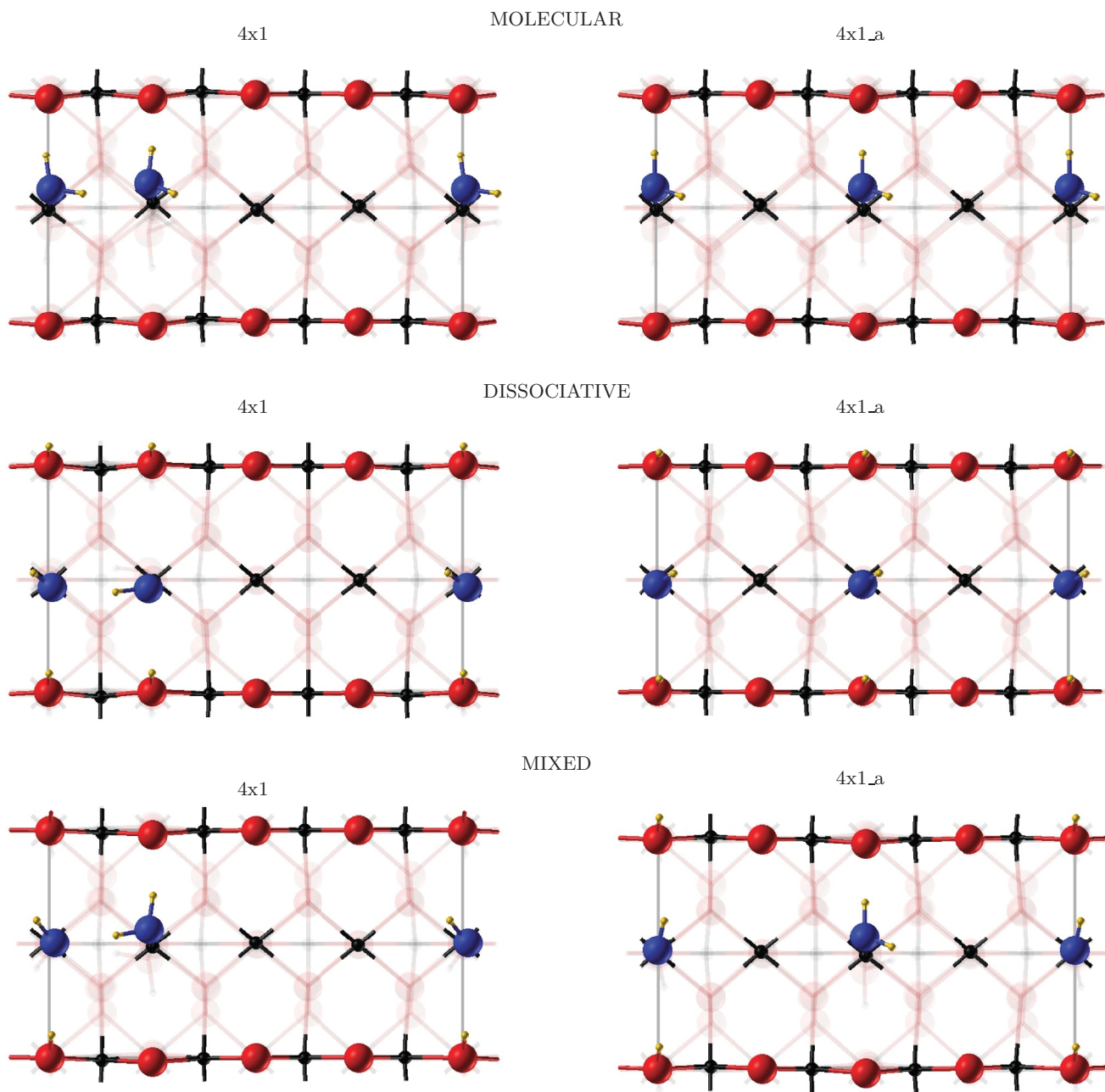


FIG. 4. (Color online) Top views of the optimized geometries of the adsorbate-substrate system illustrating two geometrical configurations in the 4×1 periodicity ($\Theta = 1/2$ ML) of each adsorption mode: molecular, dissociative, and mixed. The Ti atoms of the two uppermost atomic layers, bridging O atoms as well as those atoms belonging to the adsorbate are opaque, whereas lower layers are translucent. O, Ti, adsorbate O, and adsorbate H atoms are represented by red, black, blue, and yellow spheres, respectively. The surface unit cell in each case is represented by a grey line. If viewed in black and white: O, Ti and H atoms appear as dark grey, black and light grey spheres, respectively.

to be studied, in addition to the molecular and dissociative modes introduced previously. In Table IV, the BE for each mode as a function of coverage Θ and the corresponding supercell shape and size is reported. The adsorption occurs at the Ti_{5c} sites and is labelled as M, D, and $_$, corresponding to a molecule adsorbed molecularly and dissociatively and to an empty site, respectively. The adsorption configurations considered are then expressed in terms of M, D, and $_$, in Table IV. Two scenarios are possible: the presence of two adsorbed water species separated by an empty site or

the formation of a dimer. Three types of dimer can be identified: MM, DD, and DM. These are shown in Fig. 4 in which two geometrical configurations of each adsorption mode are illustrated at the same coverage, $\Theta = 1/2$ ML, corresponding to the 4×1 periodicity. Since the interaction between adsorbates is negligible along \mathbf{b}_{slab} , the dimer forms only along \mathbf{a}_{slab} .

At the lowest coverage considered ($\Theta = 1/2$ ML)—excluding the $2 \times 2_a$ case in which all sites along \mathbf{a}_{slab} are occupied—the dissociative mode is the most stable both with

(DD $_$) and without (D $_$) dimer formation, as can be seen in Table IV. Conversely, at higher coverages ($\Theta > 1/2$ ML), with the exception of the 1×2 periodicity,¹⁰¹ the dimers are either neighboring along \mathbf{a}_{slab} (DM) or separated by an empty site (DM $_$), and the mixed adsorption mode is the most favourable.

As discussed and documented in Sec. III A, dissociative adsorption affects the outermost atoms of the slab to a greater extent than molecular adsorption. The displacements produced as a consequence of adsorbed hydroxyls propagate further through the surface: a particular distance between dimers—8.939 Å—is required in order for the dissociative dimer to form. The interactions between adsorbates are mediated by the surface through these atomic displacements. This could provide an explanation for the dependence of adsorption mode on the coverage and arrangement of adsorbates: when dimers are neighboring along \mathbf{a}_{slab} or separated by one empty site (DM or DM $_$), the separation between them does not allow the surface distortions induced by dissociative adsorption, thus the mixed mode becomes lower in energy (see the 2×1 , 3×1 , and $2 \times 2_a$ cases in Table IV).

Increasing the separation between dimers in the dissociative mode along \mathbf{a}_{slab} from neighboring (DD) to 5.959 Å (DD $_$) to 8.939 Å (DD $_$) lowers the BE by 0.25 and 0.14 eV, respectively. The effect on the BE is much less in the mixed adsorption mode, and negligible in the molecular mode (see Table IV). The effective repulsive interactions between the dimers are lowered as the separation is increased, and since we know that the interactions between surface hydroxyls along \mathbf{a}_{slab} are more pronounced and spread over a greater distance than those between adsorbed molecules, the evidence suggests that the surface-mediated interactions are particularly significant in dissociative adsorption.

The effects of adsorbing two molecules per surface unit cell, as opposed to one, can be analyzed by comparing the two-molecule with the single-molecule binding energies. As shown in Table IV, the 1×2 periodicity is dominated by molecular adsorption. In this case, although adsorbates are neighbouring along \mathbf{a}_{slab} , the translational symmetry constraints in this direction are similar to those within the 1×1 system within the single-molecule adsorption results discussed in Sec. III A. As expected, the BE of the 1×2 periodicity for the two-molecule molecular adsorption (−1.00 eV) is marginally lower than the value for the 1×1 periodicity in the case of the single-molecule molecular adsorption (−0.98 eV), due to the decrease of symmetry constraints along \mathbf{b}_{slab} . In general, when comparing the two-molecule with the single-molecule binding energies for the same coverage, geometrical configuration and adsorption mode, the former is lower in energy by ≤ 0.03 eV. This is also owing to the greater freedom of relaxation, and links the two sets of energetics. The effect of partially breaking the symmetry in these calculations is analyzed further in Appendix B.

Water adsorption on this surface can be characterized by the favorable formation of water dimers through hydrogen bonds. The formation energy of dimers is analyzed by comparing the binding energies of the 4×1 and $4 \times 1_a$ cases ($\Theta = 1/2$ ML). In the latter, the adsorbates are separated by an empty site, while in the former they are neighboring and form a dimer, as can be seen in Fig. 4. The energy difference (Δ BE) between these configurations is attributed to the BE of the dimer with respect to two separated adsorbates. In

passing from the dissociative to the molecular to the mixed mode, the stabilisation, Δ BE, is equal to 0.04, 0.06, and 0.09 eV, respectively, per dimer formed. The benefit of having a neighboring adsorbate is therefore greatest in the mixed geometry, but is also present in the other two modes, suggesting that the order of strength of the hydrogen bond between adsorbates in a dimer is as follows: $D \cdot \cdot D < M \cdot \cdot M < D \cdot \cdot M$. Although DM forms a strong hydrogen bond and its Δ BE is largest, in this particular case (4×1), the intact water molecule deprotonates easily, resulting in DD as the most favourable dimer. The type of dimer that forms is dependent not only on the strength of hydrogen bond but also on the distance between dimers on the surface, and this emphasizes the competitive nature between direct intermolecular and surface-mediated interactions.

To summarize the adsorption energetics, the following main points can be highlighted. In the absence of neighbors along the \mathbf{a}_{slab} direction, i.e., isolated adsorbates, the dissociative mode is most favorable. The dissociative mode remains the most favorable when well-separated dimers form along \mathbf{a}_{slab} : the separation must be sufficient—8.939 Å—to allow for the structural distortion imposed by surface hydroxyls upon adsorption. Finally, the mixed adsorption mode becomes important when dimers are neighboring or separated by a short distance— ≤ 5.959 Å—as this is when the strong hydrogen bonding comes into play.

C. Electronic structure

The effects of water adsorption on the electronic structure of the rutile TiO₂(110) surface are presented here, with the aim of gaining insight into the photooxidation reaction occurring during water oxidation in water splitting systems. In particular, the electronic structure is studied in order to aid further analysis of the energetics, i.e., to elucidate the nature of chemical bonds, and to identify the position of the molecular orbitals of H₂O relative to the valence band (VB) and the conduction band (CB) of the TiO₂ surface.

In Figs. 5 and 6, the density of states (DOS) for the molecular and dissociative adsorption modes are shown for single-molecule and two-molecule adsorption, respectively. The DOS for the mixed adsorption mode is also presented in Fig. 6. For reference purposes, in both figures, the DOS for the clean surface and the isolated molecule have also been plotted.¹⁰² The DOS of the clean surface shows the contributions of the CB, upper VB, and lower VB, which are made up largely of Ti-3*d* orbitals, O-2*p* orbitals, and O-2*s* orbitals, respectively. The calculated band gap of the surface is 2.90 eV, which is in good agreement with the experimental gap of 3.03 eV (polarised optical transmission measurements).⁸⁰ Projections onto the twofold-coordinated O (bridging O) atoms show that the corresponding O-2*s* and O-2*p* states contribute primarily to the top of their respective valence bands: they are at higher energies compared to the states of threefold-coordinated O, which is consistent with a simple ionic model. With regards to the isolated water molecule, the expected four energy levels corresponding to two nonbonding and two bonding orbitals, are shown in the top panels of Figs. 5 and 6. The highest occupied orbital (1*b*₁), at −8 eV, is nonbonding and highly localized on the oxygen

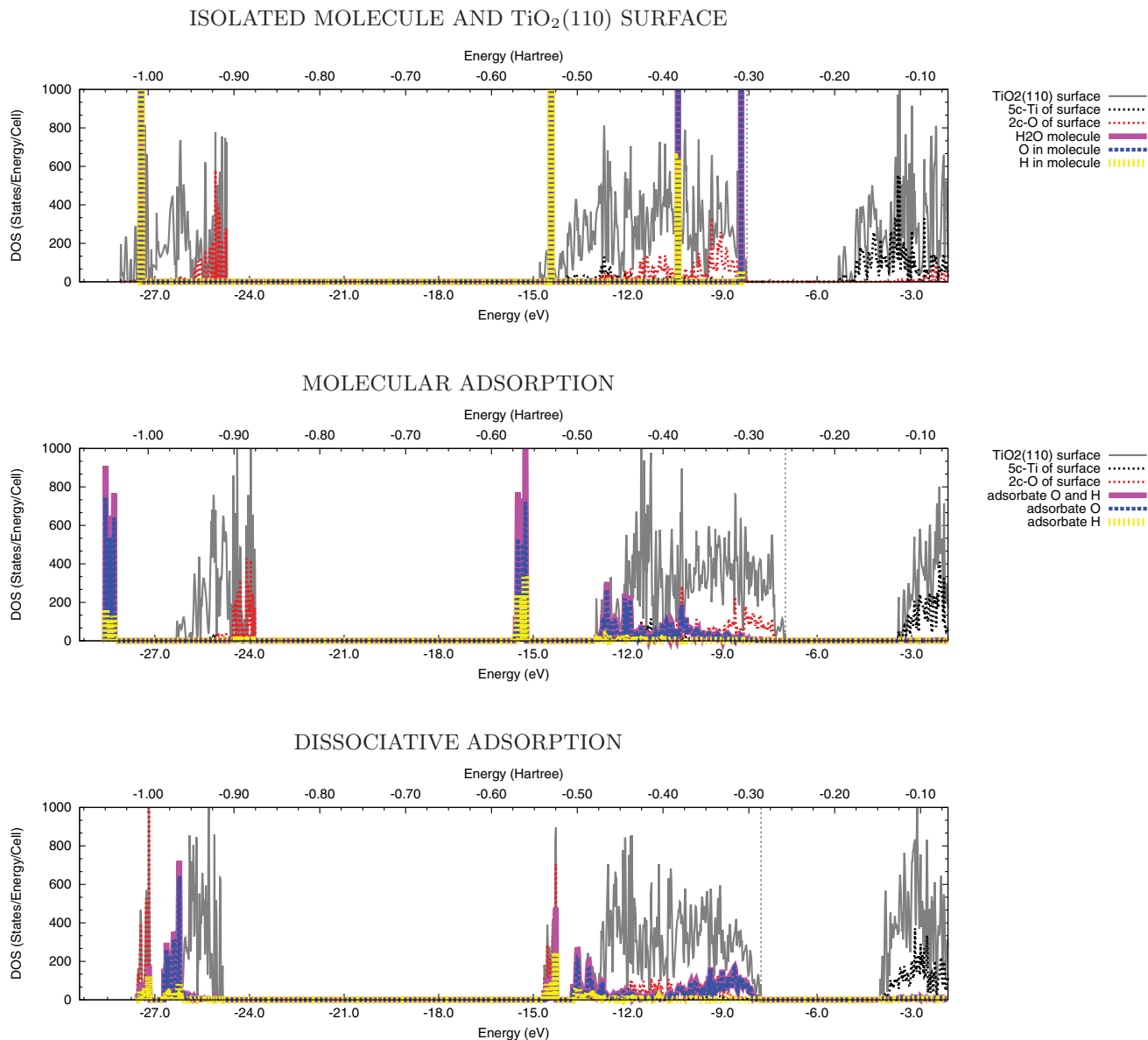


FIG. 5. (Color online) Projected density of states (DOS) for single-molecule adsorption of water onto the rutile TiO₂(110) surface (1×1 surface unit cell, $\Theta = 1$ ML). From top to bottom: superposition of the DOS for the isolated molecule and the clean surface, molecular adsorption (M), and dissociative adsorption (D). The vertical dotted line in the DOS denotes the position of the Fermi energy. All energies are referred to vacuum zero as 2D periodic boundary conditions are used: $V_{es}(z) = 0$ when $z = \infty$, where V_{es} is the electrostatic potential and z is the distance from the surface.

atom. The next orbital ($2a_1$), at -10.5 eV, is also nonbonding and mostly localized on the O atom but with some contribution from H. These two correspond to lone pair orbitals. The two lower energy molecular orbitals ($1b_2$ and $1a_1$), at -14.5 and -27.1 eV, describe two O-H bonds in the water molecule: contributions from both the O and H atoms can be seen (see Figs. 5 and 6).

The main consequences of the adsorption become evident by comparing the superposition of the DOS for the isolated molecule and the clean surface with both the molecular and dissociative cases. Firstly, there are no adsorbate states present in the band gap. Upon adsorption, an energy shift and broadening of the peaks of water occur as well as

hybridization with TiO₂ surface O- $2p$ bands. From the DOS of the molecular adsorption mode, it is evident that upon adsorption, the O- $2s$ and O- $2p$ states involved in describing the O-H bonds in the water molecule are at lower energies than the corresponding states of the isolated molecule (compare top two panels of Fig. 5); these states at ~ -15.2 and ~ -28.5 eV are characteristic of intact water molecules on the surface. In the dissociative adsorption mode, the adsorption of H onto a bridging O stabilises the O- $2s$ and O- $2p$ states of the bridging O: the resulting states at ~ -14.5 and ~ -27.5 eV characterize the bridging hydroxyls (BH). Above these BH peaks, there are the characteristic terminal hydroxyl (TH) peaks at ~ -14 and ~ -26.5 eV.

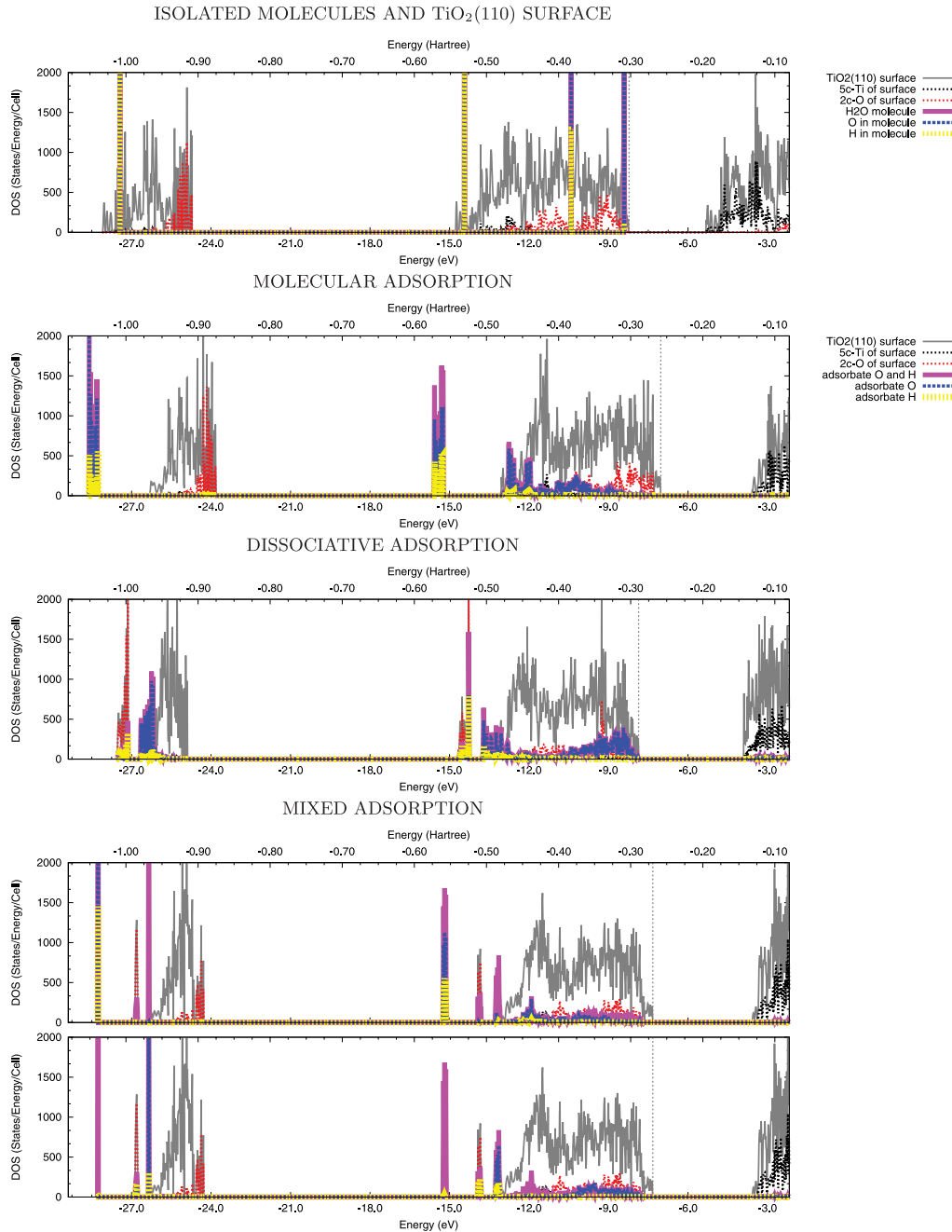


FIG. 6. (Color online) Projected density of states (DOS) for two-molecule adsorption of water onto the rutile $\text{TiO}_2(110)$ surface (2×1 surface unit cell, $\Theta = 1 \text{ ML}$). From top to bottom: superposition of the DOS for the isolated molecule and the clean surface, molecular adsorption (MM), dissociative adsorption (DD), and mixed molecular and dissociative adsorption (DM). The DOS of molecularly and dissociatively adsorbed molecules in the mixed adsorption mode have been plotted separately in order to view clearly the contributions of each. The vertical dotted line in the DOS denotes the position of the Fermi energy.

The nature of the states at the valence band maximum (VBM) is important in the development of models of photocatalytic processes. Firstly, when superimposing the DOS of the isolated molecule with that of the clean surface, the highest occupied lone pair orbital ($1b_1$), at -8 eV , lies at the top of the valence band of TiO_2 . However, in both adsorption modes, the O states associated with the lone pairs in the isolated molecule are hybridized with the TiO_2 O- $2p$ states, upon adsorption

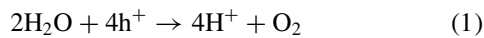
(see energy range -13.5 to -7 eV). Interestingly, this suggests that during relaxation the geometry distorts to accommodate the adsorbates, and that for both adsorption modes this results in the adsorbate O states being at similar energies to the TiO_2 O band. In molecular adsorption, the bridging O- $2p$ states are at the top of the valence band, and the highest energy adsorbate O- $2p$ states are 1.40 eV below. However, in dissociative adsorption, the top of the valence band is constituted from

adsorbate O-2*p* states (only 0.43 eV below the VBM), which are associated with the TH, and bridging O-2*p* states (0.63 eV below the VBM), involved in the formation of the BH.

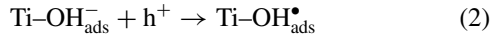
The mixed adsorption mode shows characteristics of both molecular and dissociative adsorption as expected: the contributions of the molecularly and dissociatively adsorbed molecules are illustrated in Fig. 6. The total and projected density of states for the two-molecule adsorption cases (see Fig. 6) in the molecular and dissociative modes are analogous to those for the single-molecule adsorption (see Fig. 5).

In summary, the states of the molecularly adsorbed H₂O and the two hydroxyl groups (BH and TH) of the dissociated molecule have been identified and compared with those of the isolated molecule. Energy shifts and hybridization upon adsorption have been analyzed. Alongside this, the major contributions to the valence band maximum have been determined.

This analysis of the electronic structure provides some insight into the reaction that controls the water oxidation process, known as the oxygen evolution reaction (OER),^{81–83} in TiO₂ water splitting devices. The overall equation for the oxidation of H₂O to O₂ on the TiO₂ surface is



Many of the proposed mechanisms indicate that the photooxidation of surface hydroxyls by photogenerated holes plays a crucial role.⁸⁴ This results in the formation of surface hydroxyl radicals, Ti–OH_{ads}[•]:



The coupling of two adjacent Ti – OH_{ads}[•] radicals is said to generate surface-bound hydrogen peroxide, H₂O₂. The subsequent capture and reaction of two valence band free holes with adsorbed H₂O₂ is believed to result in O₂ evolution.^{81,82,85}

An alternative mechanism has been suggested in which the reaction is initiated by the nucleophilic attack of a H₂O molecule on a surface-trapped photogenerated hole:



In this case, the radical species on the surface is supposed to oxidise TiO₂ to TiO₃. The specific steps that are said to follow are presented in Ref. 6 and 83.

The proposed mechanisms require multiple holes at a single reaction site and a build up of intermediates.⁸⁶ In TiO₂, the holes are said to accumulate at the O-2*p* states of bridging O^{2–} ions, which lie at the top of the valence band, consequently reacting with adsorbed species. Nevertheless, a complete atomic-level understanding of the reaction steps following photooxidation of surface hydroxyls has not yet been established.

The calculations presented here shed some light on these mechanisms. In molecular adsorption, there are no adsorbate states at the VBM, whereas in dissociative adsorption, O-2*p* states associated with both the TH and BH are present at the VBM. This suggests that the photogenerated holes at the surface are unlikely to react with molecularly adsorbed water, and that it is possible that they react with both terminal

and bridging hydroxyls. In order to distinguish which surface hydroxyls are more likely to react, an approach based on a combination of theory and isotopic labeling experiments is a possibility.

IV. CONCLUSIONS

Periodic hybrid-exchange density functional theory (DFT) calculations have been used to predict the structure of water on the rutile TiO₂(110) surface (Θ ≤ 1 ML). A detailed model has been developed to describe water-water and water-surface interactions at low coverages (Θ = 1/4 ML) through to 1 ML of adsorbates (Θ = 1 ML). The relaxed geometries have been analyzed and the adsorption energetics studied thoroughly. The influences of interactions that occur at the surface on the adsorption mode—molecular, dissociative or mixed—and the binding energy have been explored.

The adsorption sites are Ti_{5*c*} and both Ti_{5*c*} and O_{2*c*} for molecular and dissociative adsorption, respectively. From the energetics of adsorption, it is clear that water binds readily to the surface of rutile TiO₂(110). The outermost surface atoms undergo more pronounced structural changes upon dissociative adsorption, in comparison to molecular adsorption. In fact, we have shown that the displacements produced as a result of adsorbed hydroxyls propagate further through the surface in comparison with adsorbed water molecules.

The first important point is that only the interactions in **a**_{slab} have to be considered to predict the structure of water on this surface: the interaction model can be one-dimensional since along **b**_{slab} (6.561 Å) the level of interaction between adsorbates is negligible. Secondly, the effect on the binding energy of increasing the separation of isolated adsorbates in **a**_{slab} is more prominent in dissociative adsorption compared to molecular adsorption. The single-molecule adsorption energetics demonstrate that the repulsive interactions between the hydroxyls formed through dissociative adsorption are stronger and extend over a longer distance than those between molecularly adsorbed water. In the two-molecule results, we have shown that the formation of dimers on the surface is favorable. The hydrogen bond between adsorbates in a dimer has been characterised in order of strength: D · · D < M · · M < D · · M. In order for molecularly-adsorbed water molecules to be stable, they require hydrogen bonding to neighboring species, demonstrated by binding energies in both single-molecule and two-molecule energetics.

Although the single-molecule calculations provide an idea about the interactions between adsorbates, additional energetically-favorable adsorption structures that take into account the intermolecular interactions have been retrieved from the “two-molecule” results. These calculations have predicted that in **a**_{slab}, there are two scenarios: isolated adsorbates in the absence of neighbors [in which the dissociative mode (D) is the most stable] or the formation of one of three types of dimer: MM, DD, and DM. The dissociative mode (DD) remains the most favorable when well-separated—8.939 Å—dimers form to allow for the structural distortion imposed by surface hydroxyls upon adsorption. The mixed adsorption mode (DM) becomes important when

TABLE V. Vibrational frequencies (cm^{-1}) of the isolated water molecule. Calculated (CALC.) and scaled (SCAL.) frequencies are shown alongside two sets of experimental (EXP.) data for comparison.

Vibrational mode	Description	CALC.	SCAL.	EXP. ⁸⁷	EXP. ⁹³
ν_2	Scissoring (in-plane bending)	1610.84	1548.66	1594	1595
ν_1	Symmetric stretching	3739.52	3595.17	3656	3657
ν_3	Asymmetric stretching	3904.69	3753.97	3755	3756

dimers are neighboring or separated by a short distance. The atomic displacements produced as a consequence of adsorbed species affect the way in which neighboring molecules adsorb; this provides evidence to support the view that the interactions between adsorbates are mediated through the surface.

Furthermore, the electronic structure of the $\text{H}_2\text{O}-\text{TiO}_2$ system has been analyzed in terms of density of states. The states of the molecularly adsorbed H_2O , the bridging hydroxyl (BH), and the terminal hydroxyl (TH) have been identified, relative to the surface Ti and O states. In molecular adsorption, there are no adsorbate states at the VBM. Contrastingly, in dissociative adsorption, O-2p states associated with both the TH and BH are present at the VBM. The evidence suggests that the photogenerated holes at the surface are unlikely to react with molecularly adsorbed water, and that it is possible that they react with both terminal and bridging hydroxyls, providing some insight into the reaction that controls the water oxidation process.

This study has revealed that the preferred adsorption mode is dependent on not only coverage, but also on the arrangement of, hence the separation between, adsorbed species. At low coverage ($1/4 \text{ ML} \leq \Theta \leq 1/2 \text{ ML}$), the results have indicated that dissociative adsorption dominates; at higher coverage ($1/2 \text{ ML} < \Theta \leq 1 \text{ ML}$), the mixed mode becomes important when the intermolecular interactions are taken into account. However, it is imperative to consider the arrangement of adsorbates as well. Both dependencies (coverage and arrangement) have a significant influence on the nature of the interactions involved in the $\text{H}_2\text{O}-\text{TiO}_2$ system. The interactions can be separated into two categories: the direct attractive and repulsive interactions and the surface-mediated interactions. We have evidence to support the concept that surface-mediated interactions significantly affect the most energetically favorable adsorption structure. The interplay and

competition between these two groups of interactions could provide an explanation for the dependence of adsorption mode on the coverage and arrangement of adsorbates. This work indicates that the surface is not fully hydroxylated; when considering multilayer water, the issue then is the interaction of water with a surface containing a mixture of OH and H_2O species. The insight gained from these calculations contributes towards a better atomistic understanding of water chemistry on transition metal oxide photocatalysts, since it is the interactions and surface phenomena that determine the state of adsorbates on photocatalyst surfaces.

ACKNOWLEDGMENTS

The authors would like to thank Federico F. Sanches for participation in interesting discussions. M.P. and N.M.H. are grateful to James Durrant for useful discussions and comments. This work made use of the high performance computing facilities of Imperial College London and—via membership of the UK’s HPC Materials Chemistry Consortium funded by EPSRC (EP/F067496)—of HECToR, the UK’s national high-performance computing service, which is provided by UoE HPCx Ltd at the University of Edinburgh, Cray Inc., and NAG Ltd, and funded by the Office of Science and Technology through EPSRC’s High End Computing Programme.

APPENDIX A: ANALYSIS OF THE WATER MOLECULE: GEOMETRY AND FREQUENCIES

In this Appendix, the geometry and the vibrational frequencies of the isolated water molecule are reported and compared with previous studies^{87–93} in order to assess the quality of the computational methodology adopted. The water molecule belongs to the C_{2v} point group. The calculated bond distance, $d_{\text{OH}} = 0.964 \text{ \AA}$, is close to the experimental

TABLE VI. The binding energies (BE) per molecule of the adsorbate-substrate system with respect to the clean surface and the isolated molecule⁷⁸ are shown for relaxed geometries in single-molecule adsorption. The binding energies for molecular and dissociative adsorption modes are shown as a function of coverage, alongside the number of symmetry operators in each calculation. From this, the effect of symmetry reduction can be seen.

Supercell size	Coverage Θ	Molecular						Dissociative					
		BE/eV	S.O.	BE/eV	S.O.	BE/eV	S.O.	BE/eV	S.O.	BE/eV	S.O.	BE/eV	S.O.
1×1	1			-0.24 *	4	-0.98	2			-0.59 *	4	-0.82	2
2×1	1/2	-0.47 *	8	-0.69	4	-0.92	2	-0.87 *	8	-1.16	4	-1.21	2
3×1	1/3	-0.55 *	8	-0.70	4	-0.92	2	-1.19 *	8	-1.40	4	-1.40	2
4×1	1/4	-0.58 *	8	-0.72	4	-0.97	2	-1.29 *	8	-1.46	4	-1.46	2
1×2	1/2			-0.21 *	4	-1.06	2			-0.65	4	-0.87	2
2×2	1/4			-0.85 *	4	-1.04	2			-1.33 *	4	-1.33	2

value (0.9572 Å)^{88–90} with a percentage error of 0.75%. The calculated angle $\widehat{\text{HOH}}$ is 105.54°, which can be compared to the infrared measurement of 104.52°^{88,91} with a percentage error of 0.98%. In addition, the calculated harmonic vibrational frequencies are in good comparison with experimental data: the calculated symmetric and asymmetric stretching modes (ν_1 and ν_3) and the scissoring (in-plane bending) mode (ν_2) are comparable to two sets of experimental frequency measurements (see Table V). Harmonic vibrational frequencies computed from the dynamical matrix are expected to be greater in value than experimental data since they do not take into account the anharmonicity. The calculated frequencies can be scaled using a scaling factor,⁵⁶ $f = 0.9614$, in order to adjust for this (see Table V). The resulting scaled frequencies are in better agreement with the experimental data.

The calculated bond distance, angle, and frequencies are consistent with previous theoretical B3LYP data.⁹² It has been demonstrated that DFT calculations using the B3LYP exchange-correlation functional (combining the Becke three-parameter hybrid functional for exchange, B3, which includes a fraction of Hartree-Fock exchange, with the Lee, Yang and Parr nonlocal functional for correlation, LYP^{94–96}) provide a much better description of the water monomer compared to using other density functionals such as PP (combining the gradient correction of Perdew and Wang for exchange, and that of Perdew for correlation^{97,98}), and BP (combining the exchange functional of Becke and the Perdew functional for correlation^{98,99}), and comparable to that provided by MP2 methodology,⁹² particularly for harmonic vibrational frequencies.⁹⁰

APPENDIX B: EFFECT OF SYMMETRY CONSTRAINTS

In this section, the effects of the constraints imposed by point group symmetry on the relaxation of the atomic structure in both single-molecule and two-molecule adsorption are investigated. High and low symmetry configurations were considered. In the former, the geometry optimization was performed by preserving all the symmetry operations compatible with the adsorption of a water molecule, i.e., by

imposing the symmetry of the clean (110) surface. When defining the surface from the optimized bulk, the slab is characterized by eight symmetry operators (the identity, three rotations by 180° with the rotation along the x , y , and z axes, one horizontal and two vertical reflections with the mirror planes perpendicular to the z axis, and to the x and y axes, respectively, and the inversion). Upon adsorption of water, interactions between molecules at the surface induce a breaking of symmetry, and the number of symmetry operators is reduced. The consequences of this are discussed below.

In single-molecule adsorption, when moving from high to low symmetry cases, there is a reduction in the number of symmetry operators from eight to four and, subsequently, to two, as indicated in Table VI. For each coverage/supercell size the highest possible symmetry calculations (labelled as * in Table VI) have been discussed previously in Ref. 79. A reduction in the number of symmetry operators from eight to four (where the identity and the three rotations are kept) results in a decrease of the BE by 0.15–0.30 eV. The effect of reducing the number of symmetry operators further (from four to two symmetry operators, where the identity and one rotation with respect to one of the two periodic directions are preserved), can then be analyzed. In both the 1×1 and 1×2 cases, the BE decreases by 0.75–0.85 eV and by ~ 0.2 eV for molecular and dissociative adsorption modes, respectively: the interactions between neighboring adsorbates that induce symmetry-breaking are particularly strong. In all other cases, this reduction in symmetry results in a decrease of 0.22–0.25 eV in the molecular adsorption mode but is negligible in the dissociative adsorption mode.

In Table VII, the effect of reducing the number of symmetry operators from four to two can be seen for the two-molecule adsorption data. The trend remains the same: the BE is lowered as a result reducing the symmetry in any case by an energy within the range 0.15–0.85 eV. Conclusively, it has been made clear that the symmetry-breaking induced by the interactions between adsorbates benefits the system energetically. Although the symmetry effects discussed above are quite crucial, they have not been described in detail in previous studies^{34,42–48,66,100}.

TABLE VII. The binding energies (BE) per molecule of the adsorbate-substrate system with respect to the clean surface and the isolated molecule⁷⁸ are shown for relaxed geometries in two-molecule adsorption. Binding energies for molecular, dissociative, and mixed adsorption modes are shown as a function of coverage, alongside the number of symmetry operators in each calculation. From this, the effect of symmetry reduction can be seen. The labels a, b, and c represent different atomic configurations in the supercell, as described in Sec. III B.

Supercell size	Coverage Θ	Molecular				Dissociative				Mixed			
		BE/eV	S.O.	BE/eV	S.O.	BE/eV	S.O.	BE/eV	S.O.	BE/eV	S.O.	BE/eV	S.O.
2×1	1	-0.48	4	-0.99	2	-0.59	4	-0.85	2	-0.72	4	-1.03	2
3×1	2/3	-0.33	4	-0.95	2	-0.92	4	-1.10	2	-0.96	4	-1.15	2
4×1	1/2	-0.37	4	-0.98	2	-1.12	4	-1.24	2	-1.03	4	-1.20	2
$4 \times 1_a$	1/2	-0.49	4	-0.92	2	-1.08	4	-1.20	2	-0.90	4	-1.11	2
1×2	1	-0.24	4	-1.00	2	-0.59	4	-0.82	2	-0.40	4	-0.89	2
$2 \times 2_a$	1/2	-0.81	4	-1.06	2	-0.65	4	-0.87	2	-0.99	4	-1.09	2
$2 \times 2_b$	1/2	-0.77	4	-0.96	2	-1.16	4	-1.20	2	-0.99	4	-1.09	2
$2 \times 2_c$	1/2	-0.77	4	-0.96	2	-1.23	4	-1.23	2	-0.98	4	-1.09	2

*monica.patel10@imperial.ac.uk

- ¹B. C. H. Steele and A. Heinzl, *Nature (London)* **414**, 345 (2001).
- ²E. Serrano, G. Rus, and J. Garcia-Martinez, *Renewable Sustainable Energy Rev.* **13**, 2373 (2009).
- ³M. S. A. Abdel-Mottaleb, F. Nüesch, and M. M. S. A. Abdel-Mottaleb, *Int. J. Photoenergy* **2009**, 525968 (2009).
- ⁴M. Grätzel, *Nature (London)* **414**, 338 (2001).
- ⁵A. Listorti, J. Durrant, and J. Barber, *Nat. Mater.* **8**, 929 (2009).
- ⁶K. Juodkazis, J. Juodkazyte, E. Jelmakas, P. Kalinauskas, I. Valsiunas, P. Miccinskas, and S. Juodkazis, *Opt. Express* **18**, A148 (2010).
- ⁷N. S. Lewis and D. G. Nocera, *Proc. Natl. Acad. Sci. USA* **103**, 1572 (2006).
- ⁸M. Li, M. K. H. Leung, D. Y. C. Leung, and K. Sumathy, *Renewable Sustainable Energy Rev.* **11**, 401 (2007).
- ⁹T. Ohno, K. Saruwaka, and M. Matsumura, *New J. Chem.* **26**, 1167 (2002).
- ¹⁰P. A. M. Hotsenpiller, J. D. Bolt, W. E. Farneth, J. B. Lowekamp, and G. S. Rohrer, *J. Phys. Chem. B* **102**, 3216 (1998).
- ¹¹J. B. Lowekamp, G. S. Rohrer, P. A. M. Hotsenpiller, J. D. Bolt, and W. E. Farneth, *J. Phys. Chem. B* **102**, 7323 (1998).
- ¹²J. Pan, G. Liu, Q. Lu, and H.-M. Cheng, *Angew. Chem., Int. Ed.* **50**, 2133 (2011).
- ¹³M. Batzill, *Energy Environ. Sci.* **4**, 3275 (2011).
- ¹⁴V. E. Henrich and P. A. Cox, *The Surface Science of Metal Oxides* (Cambridge University Press, 1994).
- ¹⁵M. Ramamoorthy, D. Vanderbilt, and R. D. King-Smith, *Phys. Rev. B* **49**, 16721 (1994).
- ¹⁶U. Diebold, *Surf. Sci. Rep.* **48**, 53 (2003).
- ¹⁷A. Fujishima, *Nature (London)* **238**, 37 (1972).
- ¹⁸M. Haruta, N. Yamada, T. Kobayashi, and S. Iijima, *J. Catal.* **115**, 301 (1989).
- ¹⁹K. J. Klabunde, L. Erickson, O. Koper, and R. Richards, *Review of Nanoscale Materials in Chemistry: Environmental Applications* (American Chemical Society, 2010).
- ²⁰Y. Zhu, J. Shi, Z. Zhang, C. Zhang, and X. Zhang, *Anal. Chem.* **74**, 120 (2002).
- ²¹A. Fujishima, T. N. Rao, and D. A. Tryk, *J. Photochem. and Photobio. C* **1**, 1 (2000).
- ²²P. Fenter and N. C. Sturchio, *Prog. Surf. Sci.* **77**, 171 (2004).
- ²³R. L. Kurtz, R. Stock-Bauer, T. E. Msdey, E. Romn, and J. D. Segovia, *Surf. Sci.* **218**, 178 (1989).
- ²⁴V. E. Henrich, G. Dresselhaus, and H. J. Zeiger, *Solid State Commun.* **24**, 623 (1977).
- ²⁵S. Eriksen, P. Naylor, and R. Egddell, *Spectrochim. Acta, Part A* **43**, 1535 (1987).
- ²⁶M. B. Hugenschmidt, L. Gamble, and C. T. Campbell, *Surf. Sci.* **302**, 329 (1994).
- ²⁷M. A. Henderson, *Langmuir* **12**, 5093 (1996).
- ²⁸M. A. Henderson, *Surf. Sci.* **355**, 151 (1996).
- ²⁹D. Brinkley, M. Dietrich, T. Engel, P. Farrall, G. Gantner, A. Schafer, and A. Szuchmacher, *Surf. Sci.* **395**, 292 (1998).
- ³⁰R. Schaub, P. Thostrup, N. Lopez, E. Lægsgaard, I. Stensgaard, J. K. Nørskov, and F. Besenbacher, *Phys. Rev. Lett.* **87**, 266104 (2001).
- ³¹I. M. Brookes, C. A. Muryn, and G. Thornton, *Phys. Rev. Lett.* **87**, 266103 (2001).
- ³²S. Krischok, O. Hoff, J. Gunster, J. Stultz, D. W. Goodman, and V. Kemper, *Surf. Sci.* **495**, 8 (2001).
- ³³S. Wendt *et al.*, *Surf. Sci.* **598**, 226 (2005).
- ³⁴P. J. D. Lindan, N. M. Harrison, and M. J. Gillan, *Phys. Rev. Lett.* **80**, 762 (1998).
- ³⁵L. E. Walle, A. Borg, P. Uvdal, and A. Sandell, *Phys. Rev. B* **80**, 235436 (2009).
- ³⁶J. Goniakowski, S. Bouette-Russo, and C. Noguera, *Surf. Sci.* **284**, 315 (1993).
- ³⁷J. Goniakowski and C. Noguera, *Surf. Sci.* **330**, 337 (1995).
- ³⁸T. Bredow and K. Jug, *Surf. Sci.* **327**, 398 (1995).
- ³⁹A. Fahmi and C. Minot, *Surf. Sci.* **304**, 343 (1994).
- ⁴⁰J. Goniakowski, J. M. Holender, L. N. Kantorovich, M. J. Gillan, and J. A. White, *Phys. Rev. B* **53**, 957 (1996).
- ⁴¹J. Goniakowski and M. J. Gillan, *Surf. Sci.* **350**, 145 (1996).
- ⁴²M. Menetrey, A. Markovits, and C. Minot, *Surf. Sci.* **524**, 49 (2003).
- ⁴³C. Zhang and P. J. D. Lindan, *J. Chem. Phys.* **118**, 4620 (2003).
- ⁴⁴D. Vogtenhuber, R. Podloucky, and J. Redinger, *Surf. Sci.* **402-404**, 798 (1998).
- ⁴⁵M. Casarin, C. Maccato, and A. Vittadini, *Appl. Surf. Sci.* **142**, 196 (1999).
- ⁴⁶P. J. D. Lindan and C. Zhang, *Phys. Rev. B* **72**, 075439 (2005).
- ⁴⁷P. J. D. Lindan, N. M. Harrison, J. M. Holender, and M. J. Gillan, *Chem. Phys. Lett.* **261**, 246 (1996).
- ⁴⁸P. J. D. Lindan, J. Muscat, S. Bates, N. M. Harrison, and M. Gillan, *Faraday Discuss.* **106**, 135 (1997).
- ⁴⁹K. Sebbari, C. Domain, J. Roques, H. Perron, E. Simoni, and H. Catalette, *Surf. Sci.* **605**, 1275 (2011).
- ⁵⁰C. Sun, L. Liu, A. Selloni, G. Lu, and S. Smith, *J. Mater. Chem.* **20**, 10319 (2010).
- ⁵¹D. Muñoz, N. M. Harrison, and F. Illas, *Phys. Rev. B* **69**, 085115 (2004).
- ⁵²J. Muscat, A. Wander, and N. Harrison, *Chem. Phys. Lett.* **342**, 397 (2001).
- ⁵³G. Mallia and N. M. Harrison, *Phys. Rev. B* **75**, 165201 (2007).
- ⁵⁴N. C. Wilson, S. P. Russo, J. Muscat, and N. M. Harrison, *Phys. Rev. B* **72**, 024110 (2005).
- ⁵⁵G. Mallia, R. Orlando, M. Llunell, and R. Dovesi, in *Computational Materials Science*, edited by C. Catlow and E. Kotomin, NATO Science Series, III: Computer and Systems Sciences Vol. 187 (IOS Press, Amsterdam, 2003), pp. 102–121.
- ⁵⁶J. Scaranto, G. Mallia, S. Giorgianni, C. Zicovich-Wilson, B. Civalleri, and N. Harrison, *Surf. Sci.* **600**, 305 (2006).
- ⁵⁷F. Corà, M. Alfredsson, G. Mallia, D. Middlemiss, W. Mackrodt, R. Dovesi, and R. Orlando, in *Principles and Applications of Density Functional Theory in Inorganic Chemistry II*, edited by N. Kaltsoyannis and J. McGrady (Springer, Berlin/Heidelberg, 2004), Vol. 113, pp. 171–232.
- ⁵⁸G. C. De Fusco, B. Montanari, and N. M. Harrison, *Phys. Rev. B* **82**, 220404 (2010).
- ⁵⁹L. Ge, J. H. Jefferson, B. Montanari, N. M. Harrison, D. G. Pettifor, and G. A. D. Briggs, *ACS Nano* **3**, 1069 (2009).
- ⁶⁰G. C. De Fusco, L. Pisani, B. Montanari, and N. M. Harrison, *Phys. Rev. B* **79**, 085201 (2009).
- ⁶¹L. Liborio, G. Mallia, and N. Harrison, *Phys. Rev. B* **79**, 245133 (2009).
- ⁶²C. L. Bailey, L. Liborio, G. Mallia, S. Tomić, and N. M. Harrison, *Phys. Rev. B* **81**, 205214 (2010).
- ⁶³L. M. Liborio, C. L. Bailey, G. Mallia, S. Tomic, and N. M. Harrison, *J. Appl. Phys.* **109**, 023519 (pages 9) (2011).

- ⁶⁴E. A. Ahmad, L. Liborio, D. Kramer, G. Mallia, A. R. Kucernak, and N. M. Harrison, *Phys. Rev. B* **84**, 085137 (2011).
- ⁶⁵I. J. Bush, S. Tomic, B. G. Searle, G. Mallia, C. L. Bailey, B. Montanari, L. Bernasconi, J. M. Carr, and N. M. Harrison, *Proc. R. Soc. London A* **467**, 2112 (2011).
- ⁶⁶A. V. Bandura, D. G. Sykes, V. Shapovalov, T. N. Troung, J. D. Kubicki, and R. A. Evarestov, *J. Phys. Chem. B* **108**, 7844 (2004).
- ⁶⁷R. Dovesi *et al.*, CRYSTAL09, Università di Torino, 2010.
- ⁶⁸R. Dovesi, B. Civalieri, E. Orlando, C. Roetti, and V. R. Saunders, *Reviews in Computational Chemistry* (Wiley-VCH, Wiley, 2005), Vol. 21.
- ⁶⁹J. Muscat, PhD Thesis, University of Manchester, 1999.
- ⁷⁰J. Muscat, N. M. Harrison, and G. Thornton, *Phys. Rev. B* **59**, 2320 (1999).
- ⁷¹J. Muscat, V. Swamy, and N. M. Harrison, *Phys. Rev. B* **65**, 224112 (2002).
- ⁷²<https://bse.pnl.gov/bse/portal>
- ⁷³C. Pisani, R. Dovesi, and C. Roetti, *Hartree-Fock Ab Initio Treatment of Crystalline Systems*, Lecture Notes in Chemistry Vol. 48 (Springer Verlag, Heidelberg, 1988).
- ⁷⁴P. J. D. Lindan, N. M. Harrison, J. M. Holender, M. J. Gillan, and M. C. Payne, *Surf. Sci.* **364**, 431 (1996).
- ⁷⁵J. K. Burdett, T. Hughbanks, G. J. Miller, J. W. Richardson, and J. V. Smith, *J. Am. Chem. Soc.* **109**, 3639 (1987).
- ⁷⁶F. Labat, P. Baranek, C. Domain, C. Minot, and C. Adamo, *J. Chem. Phys.* **126**, 154703 (2007).
- ⁷⁷S. F. Boys and F. Bernardi, *Mol. Phys.* **19**, 553 (1970).
- ⁷⁸J. Scaranto, G. Mallia, and N. Harrison, *Comput. Mater. Sci.* **50**, 2080 (2011).
- ⁷⁹M. Patel, G. Mallia, L. Liborio, and N. M. Harrison, in *NSTI Nanotech 2011 Technical Proceedings* (2011), Vol. 1, pp. 779–782.
- ⁸⁰H. Tang, F. Levy, H. Berger, and P. E. Schmid, *Phys. Rev. B* **52**, 7771 (1995).
- ⁸¹R. H. Wilson, *J. Electrochem. Soc.* **127**, 228 (1980).
- ⁸²P. Salvador and C. Gutiérrez, *J. Phys. Chem.* **88**, 3696 (1984).
- ⁸³R. Nakamura and Y. Nakato, *J. Am. Chem. Soc.* **126**, 1290 (2004).
- ⁸⁴D. R. K. J. Tang, J. R. Durrant, *J. Am. Chem. Soc.* **130**, 13885 (2008).
- ⁸⁵P. Salvador, *Prog. Surf. Sci.* **86**, 41 (2011).
- ⁸⁶A. J. Cowan, J. Tang, W. Leng, J. R. Durrant, and D. R. Klug, *J. Phys. Chem. C* **114**, 4208 (2010).
- ⁸⁷S. H. Chen, K. Toukan, C. K. Loong, D. L. Price, and J. Teixeira, *Phys. Rev. Lett.* **53**, 1360 (1984).
- ⁸⁸W. S. Benedict, N. Gailar, and E. K. Plyler, *J. Chem. Phys.* **24**, 1139 (1956).
- ⁸⁹P. L. Silvestrelli and M. Parrinello, *J. Chem. Phys.* **111**, 3572 (1999).
- ⁹⁰D. A. Estrin, L. Paglieri, G. Corongiu, and E. Clementi, *J. Phys. Chem.* **100**, 8701 (1996).
- ⁹¹S. A. Clough, Y. Beers, G. P. Klein, and L. S. Rothman, *J. Chem. Phys.* **59**, 2254 (1973).
- ⁹²K. Kim and K. D. Jordan, *J. Phys. Chem.* **98**, 10089 (1994).
- ⁹³K. Kuchitsu and Y. Morino, *Bull. Chem. Soc. Jpn.* **38**, 805 (1965).
- ⁹⁴A. D. Becke, *J. Chem. Phys.* **98**, 5648 (1993).
- ⁹⁵A. D. Becke, *J. Chem. Phys.* **98**, 1372 (1993).
- ⁹⁶C. Lee, W. Yang, and R. G. Parr, *Phys. Rev. B* **37**, 785 (1988).
- ⁹⁷J. P. Perdew and Y. Wang, *Phys. Rev. B* **33**, 8800 (1986).
- ⁹⁸J. P. Perdew, *Electronic Structure of Solids '91* (Akademie Verlag, Berlin, 1991).
- ⁹⁹A. D. Becke, *Phys. Rev. A* **38**, 3098 (1988).
- ¹⁰⁰L. A. Harris and A. A. Quong, *Phys. Rev. Lett.* **93**, 086105 (2004).
- ¹⁰¹The periodic system constructed using the 1×2 supercell contains translational symmetry constraints along \mathbf{a}_{slab} , therefore does not allow interactions in this direction to be explored fully.
- ¹⁰²The Fermi levels in all surface DOS plots have not been shifted to zero, since this value is linked to the work function: an experimental observable and characteristic property of a solid surface defined as the energy required to move an electron from the Fermi level into vacuum.